Long-term behavior of the numerical solution of the cubic non-linear Scrödinger equation using Strang splitting method

Marianna Khanamiryan[a], Olavi Nevanlinna[a], Tiina Vesanen[a,*]

[a]*Department of Mathematics and Systems Analysis, Aalto University, PL 11100, 00076 Aalto, Finland*

Abstract

In the paper by U. Ascher, [1], there is an empirical observation of high frequency oscillations, which start to appear in the long-term, when solving the one dimensional cubic non-linear Schrödinger equation with Strang splitting and when the space variable is discretized with the midpoint method, suggesting that choosing the time step k be smaller than h^2, the space step squared, prevented oscillations from emerging. In this work we provide theoretical support for this evidence and derive it by using wave train analysis. The non-linear Schrödinger equation has infinitely many conservation laws, but the numerical method used here conserves only the l^2-norm, and is symplectic. The Hamiltonian is not preserved by the method and the numerical examples show that the Hamiltonian can be used as an indicator when the high frequency oscillations start to emerge.

Keywords: non-linear Schrödinger equation, conservation law, Strang splitting, midpoint method, long-time integration

*Corresponding author

Email addresses: marianna.khanamiryan[at]aalto.fi (Marianna Khanamiryan), olavi.nevanlinna[at]aalto.fi (Olavi Nevanlinna), tiina.vesanen[at]aalto.fi (Tiina Vesanen)

1. Introduction

The non-linear cubic one-dimensional Schrödinger equation (NLS) is

$$u_t = iu_{xx} + iq|u|^2u,$$

where u is a complex valued function and q is a real parameter. The equation is called focusing if $q > 0$ and defocusing if $q < 0$. The NLS appears in fiber optics, Bose-Einstein condensate theory and water wave analysis [5, 8].

The NLS is interesting from an analytical point of view, for it has an infinite number of conservation laws. In one dimension, if $q > 0$, it also admits soliton solutions. Commonly used conservation laws are the first two, L_2-norm and the Hamiltonian,

$$\frac{d}{dt}\sqrt{\int |u|^2\,dx} = 0 \quad \text{and} \quad \frac{d}{dt}\int \left(|u_x|^2 - \frac{q}{2}|u|^4\right) dx = 0$$

respectively [11].

There are numerous numerical methods that are used to approximate solutions, for example, see the list in [6, 7, 9]. In this paper, we apply Strang splitting method with the midpoint method to solve the linear space part $u_t = iu_{xx}$ and our interest lies in the long-term behavior of the approximation. The method is symplectic and preserves the l^2-norm and therefore sounds as an ideal candidate for the long time approximation.

However, this Strang splitting method resulted in high frequency oscillations in the long run, unless the time step of the approximation was chosen to be h^2, the space step squared. This was one of the examples in [1] where "marginally stable methods used on a marginally stable problems produce unexpected results". Here we derive the following estimate, $k < h^2$, for the time and step discretization, using the wave train analysis as in [10, 2].

For a small initial value function Gauckler and Lubich have proved in [3] that, among other methods, the numerical method considered here nearly preserves the l_2-norm and the Hamiltonian for a long time. In addition, though for different solver for the linear part, split-step Fourier method, the choice $k = O(h)$ was sufficient to produce good numerical results. The numerical method with the examples used here does not satisfy this criterion of smallness and the Hamiltonian is not preserved.

Instead, the Hamiltonian can be used as an indicator when the solution is deteriorating from high frequency oscillations. Checking the value of Hamiltonian or other conserved quantities was done commonly in earlier numerical analysis of the Schrödinger equation, [6, 7], but seems to be forgotten lately when geometrical integration has taken precedence. In our case the high frequency oscillations increase the derivative part $|u_x|^2$ of the Hamiltonian. However, the l_2-norm incorporated in the numerical method stays small, even if the solution is devoured by the high frequency oscillations, and thus, provides no useful information concerning the solution.

The paper is organized as follows: In Section 2 we present the numerical method and the results from the wave train analysis, see [10] for additional details. In Section 3, the behavior of the Hamiltonian is analyzed and numerical results from two different initial value functions are given. Section 4 contains the conclusions.

2. Conditions for instabilities

The NLS admits wave train solutions,

$$\mathring{u}(x,t) = a\ \exp i(kx - \omega t), \tag{1}$$

if $\omega = k^2 - q|a|^2$. Let the wave train solution $\mathring{u}$ is perturbed to,

$$u(x,t) = \mathring{u}(x,t)(1 + \varepsilon(x,t)),$$

where $|\varepsilon|^2 \ll 1$, and assume periodic boundary conditions on an interval of length L. Then the n^{th} mode of the Fourier expansion of the perturbation ε will grow exponentially, if

$$0 < \left(\frac{2\pi n}{L}\right)^2 < 2q|a|^2,$$

see for example [10]. This analytical instability can only occur if $q > 0$ and it concerns only the low frequency modes.

2.1. The numerical method

We write the non-linear Schrödinger equation

$$iu_t + u_{xx} + q|u|^2 u = 0 \tag{2}$$

as a sum of the linear and non-linear parts,

$$u_t = i\mathcal{L}u + i\mathcal{N}u,$$

where

$$\mathcal{L}u := u_{xx} \quad \text{and} \quad \mathcal{N}(u) := q|u|^2.$$

The right hand side of the formula

$$u(x, t + k) \approx \exp\ ik(\mathcal{L} + \mathcal{N}(u)) \cdot u(x, t),$$

is Strang split as,

$$\exp\ ik(\mathcal{L} + \mathcal{N}(u)) \cdot u(x, t) \approx \exp\ i\frac{k}{2}\mathcal{L} \cdot \exp\ i\,k\,\mathcal{N}(u) \cdot \exp\ i\frac{k}{2}\mathcal{L} \cdot u(x, t),$$

where k denotes the time step. The splitting is second order accurate.

If the approximation of $u(x, t)$ is denoted by $U(x, t)$ we can write the steps of the numerical method with help of quantities V^m and W^m:

$$\begin{aligned} V^m &:= \exp\ i\frac{k}{2}\mathcal{L} \cdot U^m, \\ W^m &:= \exp\ i\,k\,\mathcal{N}(V^m) \cdot V^m, \\ &\text{and} \\ U^{m+1} &:= \exp\ i\frac{k}{2}\mathcal{L} \cdot W^m, \end{aligned}$$

where U^m is the approximation at the time mk.

From the numerical point of view the second step is computed as

$$W_j^m = \exp\,(iqk|V_j^m|^2) \cdot V_j^m, \tag{3}$$

where j refers to the approximation at the space point jh. For the first and third step we use the midpoint method rule:

$$\frac{V^m - U^m}{2} = \frac{i}{2}\left[\Delta_h\ V^m + \Delta_h\ U^m\right], \tag{4}$$

and

$$\frac{U^{m+1} - W^m}{2} = \frac{i}{2}\left[\Delta_h\ U^{m+1} + \Delta_h\ W^m\right]. \tag{5}$$

These can be written in matrix form as

$$(I - i\frac{r}{2}S)V^m = (I + i\frac{r}{2}S)U^m, \tag{6}$$

and

$$(I - i\frac{r}{2}S)U^{m+1} = (I + i\frac{r}{2}S)W^m, \tag{7}$$

where

$$r = \frac{k}{2h^2}.$$

Here I is the $N \times N$ identity matrix and S is $N \times N$ matrix of the form,

$$\begin{pmatrix} -2 & 1 & \cdot & \cdot & \cdots & 1 \\ 1 & -2 & 1 & \cdot & \ldots & \cdot \\ \cdot & 1 & -2 & 1 & \ldots & \cdot \\ \vdots & & & \ddots & & \vdots \\ \cdot & & & 1 & -2 & 1 \\ 1 & & \cdots & & 1 & -2 \end{pmatrix}.$$

This method conserves the L_2-norm in the discrete sense:

$$\sum_j |U_j^m|^2 h = \sum_j |U_j^{m+1}|^2 h.$$

2.2. Analysis of the numerical method

Instability of the wave train solution is investigated following ideas presented in [10]. Due to three steps ($U^m \to V^m \to W^m \to U^{m+1}$) in the numerical method the analysis is a lot more complicated compared to the analysis of the two step sequential splittig in [10].

We use the test subject:

$$\mathring{U}^m := a \ \exp(iq|a|^2 mk), \tag{8}$$

which is perturbed to

$$U_j^m = \mathring{U}^m(1 + \varepsilon_j^m), \tag{9}$$

where $|\varepsilon_j^m|^2 \ll 1$.

The first step (6) of the iteration will simply multiply the $\mathring{U}^m$ by a constant: if $\mathring{V}^m$ denotes the result of the equation (6) after substituting (9) into it, then

$$\begin{aligned} -i\frac{r}{2}\mathring{V}_{k-1}^m + (1+ir)\mathring{V}_k^m - i\frac{r}{2}\mathring{V}_{k+1}^m \\ = \quad i\frac{r}{2}\mathring{U}_{k-1}^m + (1-ir)\mathring{U}_k^m + i\frac{r}{2}\mathring{U}_{k+1}^m \\ = \quad i\frac{r}{2}\mathring{U}^m + (1-ir)\mathring{U}^m + i\frac{r}{2}\mathring{U}^m \\ = \quad \mathring{U}^m. \end{aligned}$$

This can be summarized in matrix notation,

$$(I - i\frac{r}{2}S)\mathring{V}^m = \mathring{U}^m.$$

To solve the equation

$$\mathring{V}^m = (I - i\frac{r}{2}S)^{-1}\mathring{U}^m$$

we notice that the sum of the row elements of the inverse matrix $(I - i\frac{r}{2}S)^{-1}$ is one and the components of $\mathring{U}^m$ are all the same so the result is

$$\mathring{V}^m = \mathring{U}^m.$$

Thus we can write,

$$V_j^m = \mathring{U}^m(1 + \alpha_j^m), \tag{10}$$

for the result of the equation (6).

Substituting (9) and (10) into the equation (6), we see that the relation between the variations ε_j^m and α_j^m is

$$\alpha_j^m - i\frac{k}{4}\mathcal{L}_h\alpha_j^m = \varepsilon_j^m + i\frac{k}{4}\mathcal{L}_h\varepsilon_j^m, \tag{11}$$

where

$$\mathcal{L}_h\varepsilon_j^m = \frac{\varepsilon_{j+1}^m - 2\varepsilon_j^m + \varepsilon_{j-1}^m}{h^2}.$$

Inserting the result (10) into the second step (3) of the iteration and discarding all second order terms of α_j^m gives the following,

$$W_j^m = \mathring{U}^{m+1}(1 + (1 + ikq|a|^2)\alpha_j^m + ikq|a|^2\alpha_j^{m*}). \tag{12}$$

If this is abbreviated to,

$$W_j^m = \mathring{U}^{m+1}(1 + \beta_j^m),$$

where

$$\beta_j^m = (1 + ikq|a|^2)\alpha_j^m + ikq|a|^2\alpha_j^{m*},$$

then the relation between the variations β_j^m and ε_j^{m+1} is

$$\varepsilon_j^{m+1} - i\frac{k}{4}\mathcal{L}_h\varepsilon_j^{m+1} = \beta_j^m + i\frac{k}{4}\mathcal{L}_h\beta_j^m. \tag{13}$$

Changing the time from $(m+1)k$ to mk in (13) and summing the equations (11) and (13) gives ε_j^m in terms of α_j^m and β_j^{m-1}:

$$2\varepsilon_j^m = \alpha_j^m + \beta_j^{m-1} + i\frac{k}{4}\mathcal{L}_h(\beta_j^{m-1} - \alpha_j^m). \tag{14}$$

Substituting $U_j^{m+1} = \mathring{U}^{m+1}(1 + \varepsilon_j^{m+1})$ and (12) into the third step (7) results in

$$\varepsilon_j^{m+1} - i\frac{k}{4}\mathcal{L}_h\varepsilon_j^{m+1} = (1 + i\frac{k}{4}\mathcal{L}_h)\alpha_j^m + ikq|a|^2(1 + i\frac{k}{4}\mathcal{L}_h)(\alpha_j^m + \alpha_j^{m*}). \tag{15}$$

Substituting (14) and all recurring β_j^m-terms into (15) we finally obtain and equation which relates α^{m+1}-terms with α^m-terms:

$$\begin{aligned}
&\alpha_j^{m+1} - \frac{kr}{8}\mathcal{L}_h\alpha_{j-1}^{m+1} + \left(\frac{kr}{4} - i\frac{k}{2}\right)\mathcal{L}_h\alpha_j^{m+1} - \frac{kr}{8}\mathcal{L}_h\alpha_{j+1}^{m+1} \\
&= (1 + ikq|a|^2)(1 + i\frac{k}{2}\mathcal{L}_h)\,\alpha_j^m + ikq|a|^2(1 + i\frac{k}{2}\mathcal{L}_h)\,\alpha_j^{m*} \\
&- \frac{kr}{8}(1 + ikq|a|^2)\mathcal{L}_h\alpha_{j-1}^m - i\frac{k^2rq|a|^2}{8}\mathcal{L}_h\alpha_{j-1}^{m*} \\
&+ \frac{kr}{4}(1 + ikq|a|^2)\mathcal{L}_h\alpha_j^m + i\frac{k^2rq|a|^2}{4}\mathcal{L}_h\alpha_j^{m*} \\
&- \frac{kr}{8}(1 + ik|a|^2)\mathcal{L}_h\alpha_{j+1}^m - i\frac{k^2rq|a|^2}{8}\mathcal{L}_h\alpha_{j+1}^{m*}.
\end{aligned} \tag{16}$$

Suppose that the perturbation α_j^m to be periodic on the interval $[-\frac{L}{2}, \frac{L}{2}]$ and $h = L/N$, $j = -N/2, \ldots, N/2$, $x_j = jh$. Then we can express α_j^m as a discrete Fourier series,

$$\alpha_j^m = \sum_{n=-N/2}^{N/2-1} \hat{\alpha}_n^m exp(i\mu_n x_j), \tag{17}$$

with frequencies,

$$\mu_n = \frac{2\pi n}{L}.$$

Substituting (17) into (16) yields

$$\begin{pmatrix} \hat{\alpha}_n^{m+1} \\ \hat{\alpha}_{-n}^{m+1*} \end{pmatrix} = B_n \begin{pmatrix} \hat{\alpha}_j^m \\ \hat{\alpha}_{-j}^{m*} \end{pmatrix}, \quad n = -N/2 \ldots N/2 - 1, n \neq 0$$

where the matrix B_n is quite similar as the A_n in [10], page 492,

$$B_n = \begin{pmatrix} d_n^2\,(1 + i\frac{k}{2}q|a|^2) & d_n^2\,i\frac{k}{2}q|a|^2 \\ -d_n^{-2}\,i\frac{k}{2}q|a|^2 & d_n^{-2}\,(1 - i\frac{k}{2}q|a|^2) \end{pmatrix},$$

where

$$d_n = \frac{1 + irs_n}{1 - irs_n}, \quad r = \frac{k}{2h^2}, \quad s_n = \cos\mu_n h - 1.$$

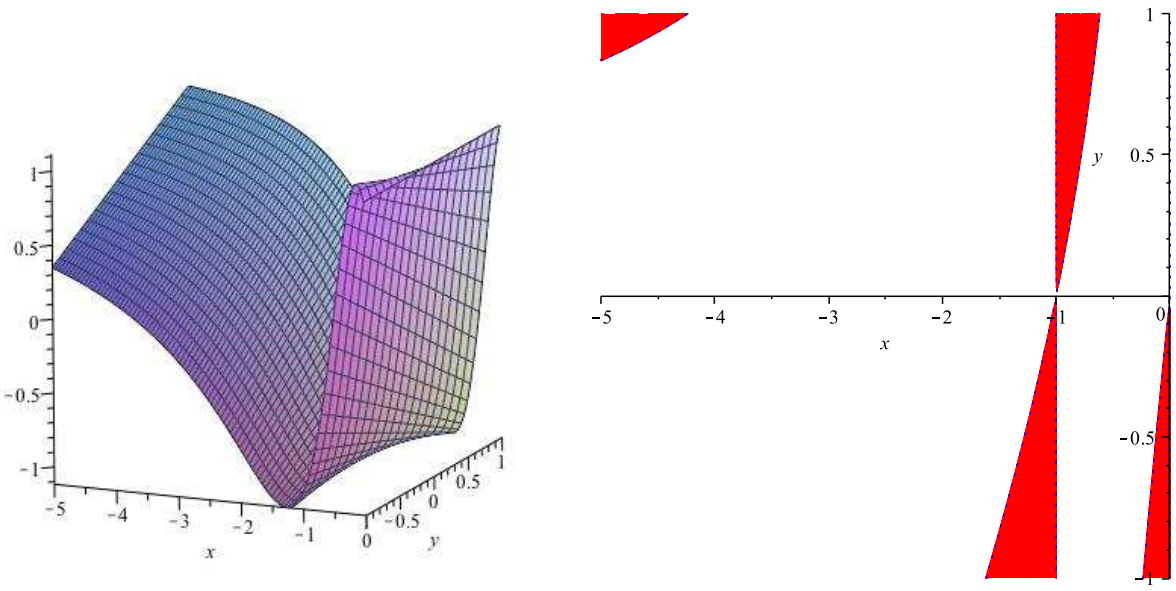

Figure 1: The graph of function $f(x,y) = (1 - 6x^2 + x^4 - 2yx(x^2 - 1))/(1 + x^2)^2$ is on the left hand side. On the right hand side are the areas where $|f(x,y)| > 1$.

The eigenvalues λ_n of B_n are of the same form as of A_n:

$$\lambda_n = \gamma_n \pm (\gamma_n^2 - 1)^{1/2}$$

except that

$$\gamma_n = \frac{1 - 6r^2 s_n^2 + r^4 s_n^4 - 2kq|a|^2 r s_n (r^2 s_n^2 - 1)}{(1 + r^2 s_n^2)^2}.$$

The intermediate solution V^m becomes unstable if $|\lambda_n| > 1$. This is equivalent to $|\gamma_n| > 1$ which is easier to examine. The function

$$f(x) = \frac{1 - 6x^2 + x^4 - 2yx(x^2 - 1)}{(1 + x^2)^2}$$

is plotted to the left hand side of the Figure 1. On the right hand side are the areas where $|f(x,y)| > 1$.

The variable x was a replacement for rs_n with dependence on k, h, and n, and values of x that interest us, are on the interval $[-2r, 0] = [-k/h^2, 0]$. The variable y was a replacement for $kq|a|^2$, so the analysis is not that straightforward. However, the sign y corresponds to the sign of q, and values near y-axis correspond to the smaller n values. In addition, the line $x = -1$ is an important threshold: if $-k/h^2$ lies on the left hand side of it, there is no way to avoid the case $|\gamma_n| > 1$, unless k is made very small. This gives a qualitative explanation to the observation in [1], that if k is chosen smaller than h^2, then the numerical method does not exhibit high frequency oscillations.

Thus, the Figure 1 suggests that for the negative values of q, the low frequency modes are unstable. The other area for instabilities lies on the left hand side of the line $x = -1$. Thus choosing $k < h^2$ guarantees that no high frequency oscillations should take place. For $q > 0$ there is two areas for instabilities, one on the right hand side of the line $x = -1$ and one further the negative x-axis. For positive q, it should be possible to prevent the high frequency oscillations to emerge, if k and h are chosen so that all possible values of rs_n lie on the right hand side of the instability area near $x = -1$.

The results of the following, more thorough, analysis are collected to the Table 1.

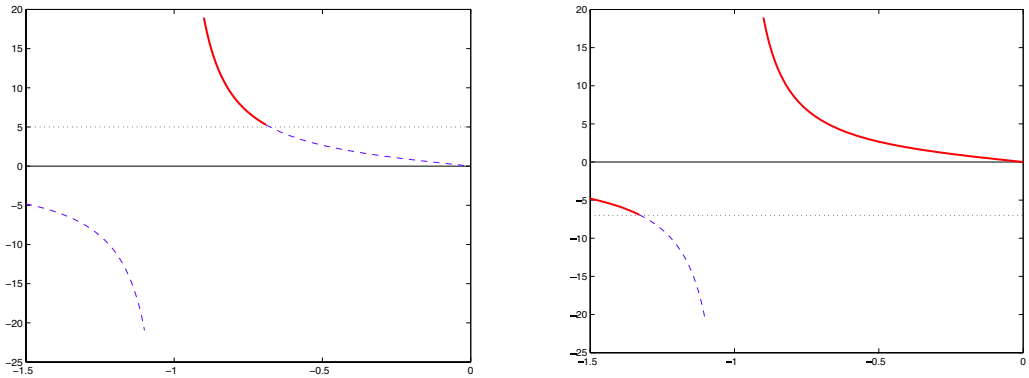

Figure 2: The graph of function $f(x) = 4x/(x^2 - 1)$ with cases $-kq|a|^2 > 0$, and $-kq|a|^2 < 0$.

2.2.1. The case $\gamma_n > 1$

The inequality $\gamma_n > 1$ is equivalent to,

$$-kq|a|^2(r^2 s_n^2 - 1) < 4rs_n. \tag{18}$$

If $rs_n < -1$, which can only happen if $k > h^2$, and if $|n|$ is large enough, then (18) is equivalent to

$$-kq|a|^2 < \frac{4rs_n}{r^2 s_n^2 - 1}.$$

From Figure 2 we see that if x, in place of rs_n, is less that -1 then instabilities are possible only if $-kq|a|^2 < 0$ and thus if q is positive. Then for the modes with $rs_n < -1$, the appearance of instabilities can be prevented if

$$-kq|a|^2 \geq \frac{4rs_{N/2}}{r^2 s_{N/2}^2 - 1},$$

or equivalently

$$k \leq h\sqrt{4/q|a|^2 + h^2}. \tag{19}$$

If $k < h^2$, or n is small enough in the case $k > h^2$, then $-1 < rs_n < 0$ and $r^2 s_n^2 - 1 < 0$. In this case (18) is equivalent to,

$$-kq|a|^2 > \frac{4rs_n}{r^2 s_n^2 - 1},$$

If $q > 0$ then $-kq|a|^2 < 0$, so all the modes are stable according to (18). For $q < 0$ there are low frequency instabilities unless

$$-kq|a|^2 \leq \frac{4rs_1}{r^2 s_1^2 - 1}. \tag{20}$$

If N is large, say greater than 100, we can approximate $s_1 = \cos(2\pi h/L) - 1$ by $-2\pi^2 h^2/L^2$. Then the inequality (20) is equivalent to

$$h^4 \geq \frac{L^2}{4q|a|^2\pi^4}\left(4\pi^2 + q|a|^2 L^2\right).$$

The right hand size of this inequality is negative if $-q|a|^2 < 4\pi^2/L^2$.

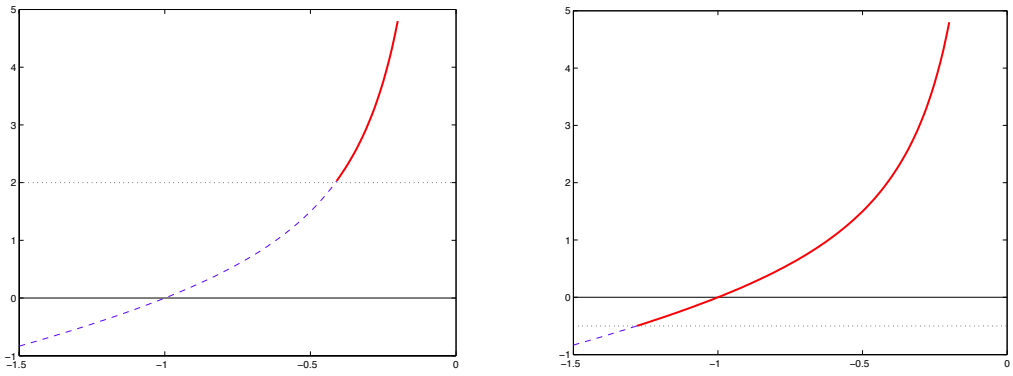

Figure 3: The graph of function $f(x) = x - 1/x$ with cases $kq|a|^2 > 0$, and $kq|a|^2 < 0$.

2.2.2. The case $\gamma_n < -1$

The inequality $\gamma_n < -1$ is equivalent to

$$(1 - r^2 s_n^2)(1 + kq|a|^2 r s_n - r^2 s_n^2) < 0. \tag{21}$$

If $rs_n < -1$ then the inequality (21) is equivalent to

$$kq|a|^2 < rs_n - \frac{1}{rs_n},$$

and from the Figure 3 we can see that there can be high frequency instabilities only if $q < 0$ under the assumption $x = rs_n < -1$. The instabilities are prevented if

$$kq|a|^2 \geq rs_n - \frac{1}{rs_n} \tag{22}$$

for all n such that $rs_n < -1$. Let m be the smallest such n. If $rs_m = -1 - \varepsilon$ then equation (22) is equivalent to $k \leq 2\varepsilon/(-q|a|^2)$. If $|m|$ is near $N/4$ we can approximate ε by the largest possible step, approximately r times the size of the angle step, $r \cdot 2\pi h/L = \pi k/hL = \pi k/h^2 N$. This gives only a restriction to the space step:

$$h \leq \frac{2\pi}{-q|a|^2 L}.$$

If $-1 < rs_n < 0$, then $1 - r^2 s_n^2 > 0$ and (21) is equivalent to

$$kq|a|^2 > rs_n - \frac{1}{rs_n}.$$

Thus the inequality (21) implies that there are no instabilities if $q < 0$. If $q > 0$, we must have

$$kq|a|^2 \leq rs_{N/2} - \frac{1}{rs_{N/2}}$$

to prevent the instabilities to occur. This condition is equivalent to,

$$k < \frac{h^2}{\sqrt{1 + q|a|^2 h^2}} \quad < h^2. \tag{23}$$

Thus choosing k according to the inequality (23), i.e. namely than h^2 guarantees that no instabilities if $q > 0$.

		No instabilities if
$q > 0,$	$-1 < rs_n < 0:$	$k < h^2/\sqrt{1 + q\|a\|^2h^2}$
	$rs_n < -1:$	$k < h\sqrt{4/q\|a\|^2 + h^2}$
$q < 0,$	$-1 < rs_n < 0:$	(approx.) $-q\|a\|^2 < 4\pi^2/L^2$ (only low freq.)
	$rs_n < -1:$	(approx.) $h \leq 2\pi/(-q\|a\|^2L)$

Table 1: Summary of all cases.

2.2.3. Conclusions

For $q > 0$ we require a stricter condition

$$k < \frac{h^2}{\sqrt{1 + q|a|^2h^2}}$$

to keep the any oscillations from appearing.

For $q < 0$, the analysis gives only constant, and approximate, restrictions,

$$-q|a|^2 < \frac{4\pi^2}{L^2}$$

for low frequency oscillations and

$$h \leq \frac{2\pi}{-q|a|^2L}$$

for high frequency oscillations in the case $k > h^2$. Thus, the choice $k < h^2$ is sufficient to avoid the high frequency oscillations in the long-term.

2.3. Splitting the non-linear part first

The Strang splitting could also be done with the non-linear part first:

$$\exp\ ik(\mathcal{L} + \mathcal{N}(u)) \cdot u(x,t) \approx \exp\ i\,\frac{k}{2}\,\mathcal{N}(u) \cdot \exp\ i\,k\,\mathcal{L} \cdot \exp\ i\,\frac{k}{2}\,\mathcal{N}(u) \cdot u(x,t).$$

Two consecutive non-linear half steps combine into one whole step. Thus the analysis and results are similar to the sequential splitting in [10].

3. Numerical results

3.1. The role of the Hamiltonian

The numerical method preserves only the one discrete version of them, the ℓ^2-norm. The relative difference of the ℓ^2-norm, i.e. the difference between the norm at time t minus the norm in the beginning at $t = 0$, stayed below 10^{-10} in all our examples, even if the solution was beyond recognition. The discrete version of the Hamiltonian,

$$\sum_{i=1}^{N-1} \frac{|u_{i+1} - u_i|^2}{h^2} - \frac{q}{2}\sum_{i=1}^{N} |u_i|^4, \tag{24}$$

instead, indicated nicely some of the errors of the numerical method made.

For example, when using the soliton initial value function fro the case $q = 1$, see Figure 4,

$$u(0,x) = e^{ix/2}\,\mathrm{sech}(x/\sqrt{2}) + e^{i(x-25)/20}\,\mathrm{sech}((x-25)/\sqrt{2}), \tag{25}$$

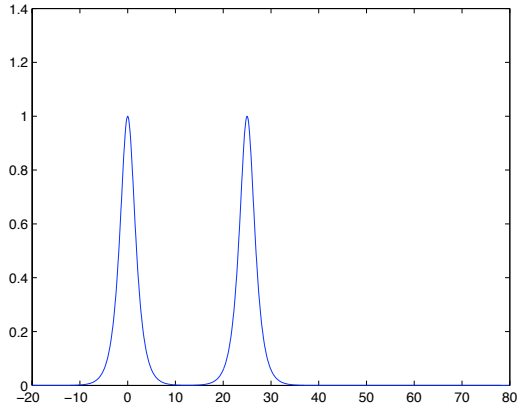

Figure 4: The initial value function $u(0,x) = e^{ix/2}\,\mathrm{sech}(x/\sqrt{2}) + e^{i(x-25)/20}\,\mathrm{sech}((x-25)/\sqrt{2})$ consists of two solitons moving right at different speeds.

with periodic boundary conditions on the interval $[-20, 80]$ from [4, 1], the solution should present two solitons, with their form preserved at all times, moving to the right with different speeds and coalescing almost periodically.

Using $h = 0.1$ and $k = 0.025$, (which equals $h/4$), the discrete Hamiltonian (24) is calculated for each approximation and difference of the value of the Hamiltonian at the time t and $t = 0$ plotted in Figure 6 for the time interval $[0, 300]$. From this we can see that numerical method cannot keep up with the fast interaction of the solitons. This shows as a small difference in the position of the solitons, as can be seen from the left hand side of Figure 5 and small increase in the relative difference of the Hamiltonian after the interaction as can be seen from Figure 9. However, the phase of u has much greater difference between the solutions as can be seen on the right of the Figure 5. The size of the space step h used is 0.1 and the values for k are h, $h/2$, $h/4$ and h^2. Here the solution for $k = h$ is already showing some high frequency oscillation.

Returning to the case $h = 0.1$ and $k = 0.025$, at $t = 900$ small oscillations start to show, see Figure 7. By this time the difference in the Hamiltonian has grown to 4.09. By the time $t = 1200$ the oscillations overtake the solution completely as can be seen from Figure 8. By then the difference in the Hamiltonian is 2170.

The Figure 9 depicts the usual behavior of the Hamiltonian in the oscillatory case. The inability of the numerical method to approximate the soliton interactions correctly increases the error in the Hamiltonian a little by little until the high frequency oscillations start to grow and finally take over the solitons. If the length of the interval and thus, the frequency of the interactions were approximately halved, it took approximately twice the time for the solution to deteriorate.

3.2. Numerical examples

Our analysis of the numerical method concerned only a single frequency. The meaning of a in the condition (23) is vague in the case of a more general initial value function, simply because there are multitude of modes, and even the unstable modes do not grow in an unlimited way due to the stabilizing and non-linear features of the Scrödinger equation. However, in the following examples, the choice of k to be a little smaller than h^2 results high frequency oscillation free numerical runs.

3.2.1. The soliton example from [4] and [1]

The initial value function (25) depicts two solitons with height 1 and with speeds of 1 and 1/10. The absolute value of $u(0,x)$ is plotted in Figure 4.

In the discrete Fourier transform of $u(0,x)$, the maximum size of a frequency component $|a|$ is 4.44 if $h = 0.1$. Thus if we set $|a|h$ equal to 0.444 (this is true for other values of h as well) in the (23) then the condition gives $k < 0.914 \cdot h^2 = 0.00914$. Compared to the numerical results, this scenario is too strict, see Table 2, or else the instability does not occur unless t is larger than the values tested here.

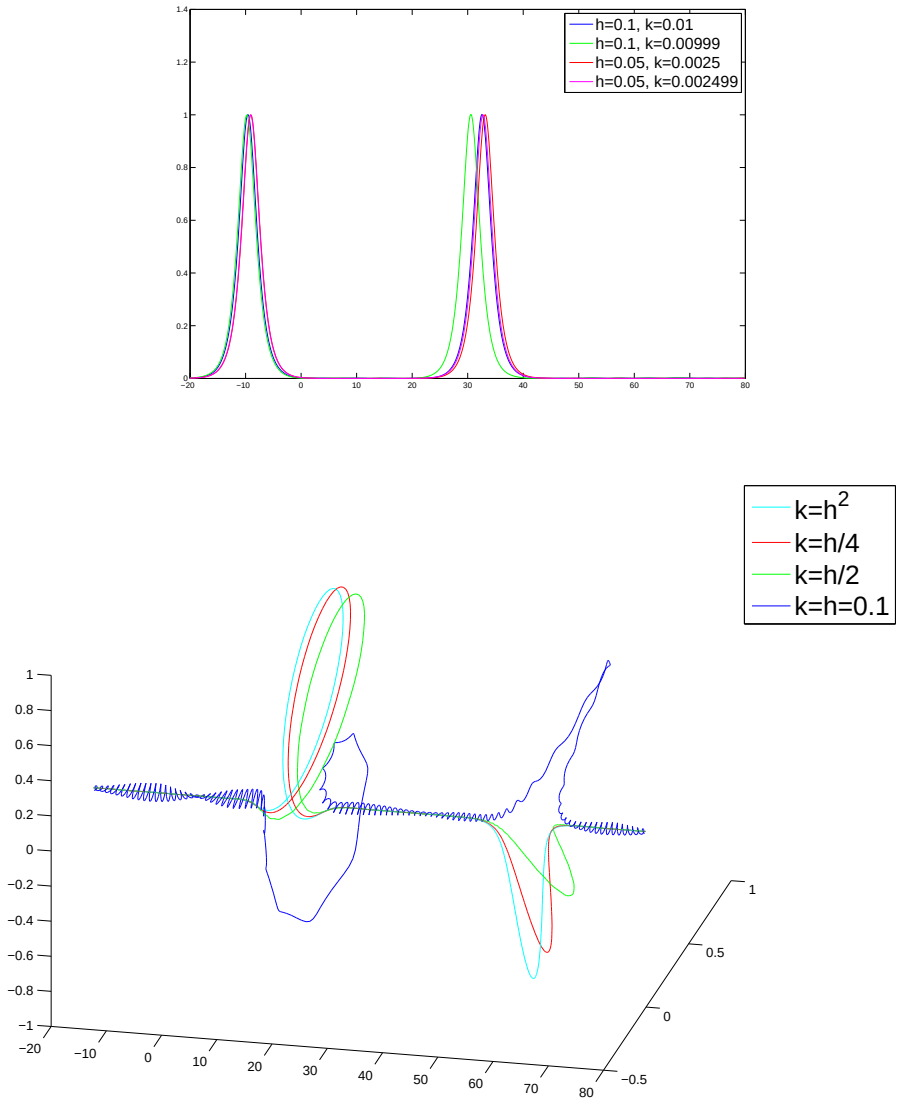

Figure 5: The approximation for $u(1000, x)$ for four different pairs of h and k is plotted in the upper image. The pairs were chosen from the cases where there were no high frequency oscillations visible at the time $t = 1000$. Below, the phase information is also shown for the case $h = 0.1$ and four different values for k at the time $t = 500$. Here the biggest choice $k = h$ results visible oscillations already at $t = 500$.

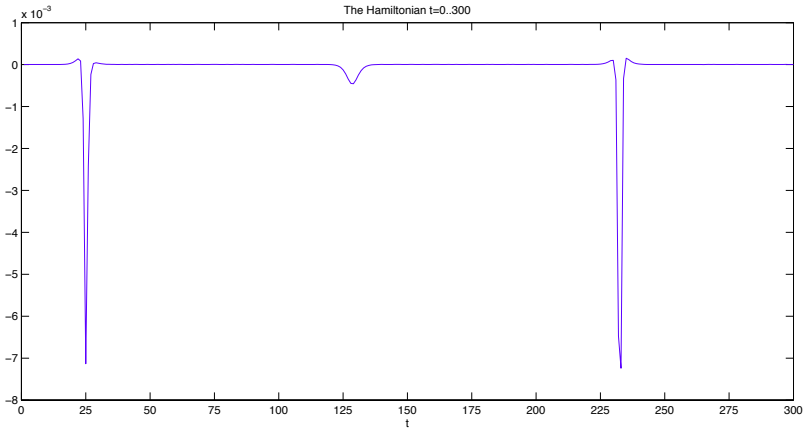

Figure 6: The value of the discrete Hamiltonian at the time interval $[0, 300]$. The interaction of the coalescing solitons happen too fast for the numerical approximation to keep up and this shows as small dents of size -7×10^{-3} in the graph of the Hamiltonian.

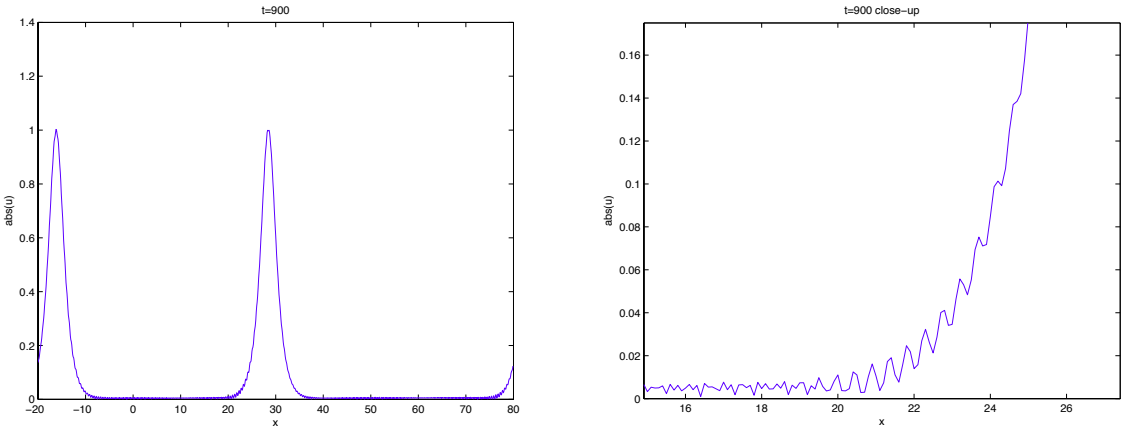

Figure 7: The approximation at the time $t = 900$ starts to show small oscillation as can be seen at least from the close-up at the right hand side. The difference in the Hamiltonian at time $t = 900$ and $t = 0$ has grown to greater than 4.

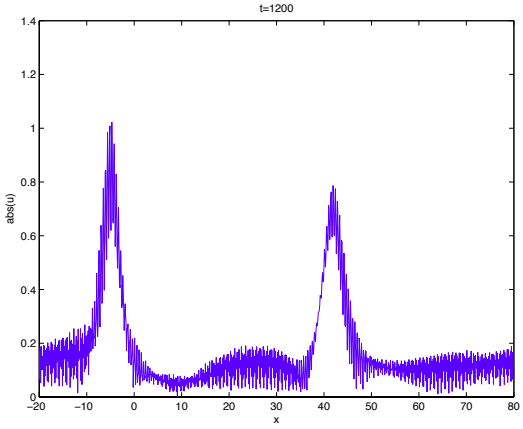

Figure 8: The approximation at the time $t = 1200$ has deteriorated. The difference in the Hamiltonian has grown grater than 2000.

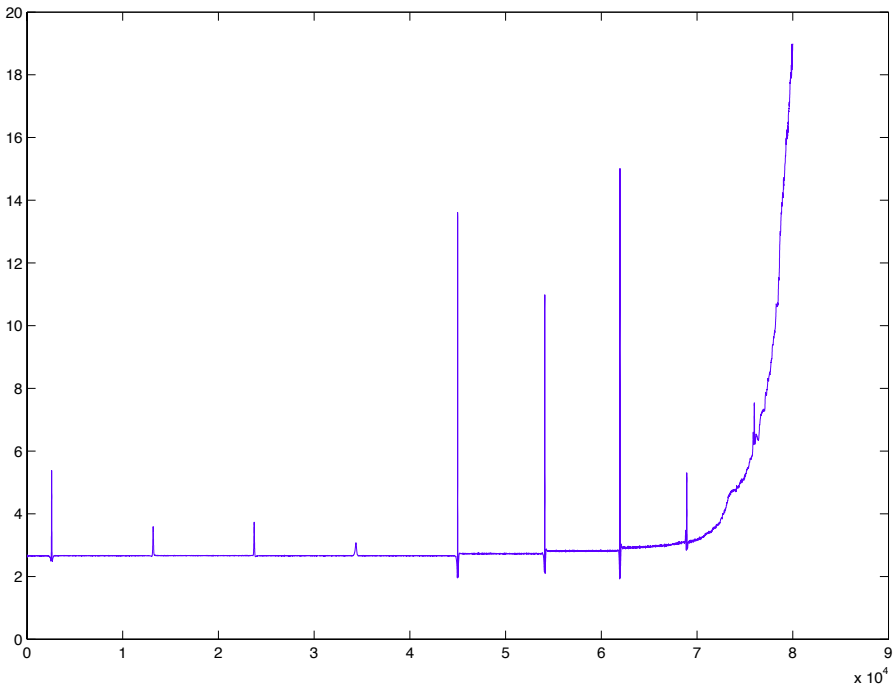

Figure 9: The Hamiltonian of the case $q = 10$ in the NLS and $k = h = 0.1$. The time interval is $[0, 800]$. For the soliton interaction causes the spikes.

Space step $h = 0.1$	
k	Stop
0.1 (= h)	418
0.05 (= $h/2$)	505
0.025 (= $h/4$)	808
0.01 (= h^2)	2133
0.009999	1652
0.00999	4356
0.0099	> 40000

Space step $h = 0.05$	
k	Stop
0.05 (= h)	538
0.025 (= $h/2$)	1344
0.0125 (= $h/4$)	675
0.0025 (= h^2)	2011
0.002499	> 10000
0.0024	> 12000

Space step $h = 0.01$	
k	Stop
0.01 (= h)	610
0.005 (= $h/2$)	486
0.0025 (= $h/4$)	> 5000

Table 2: The constant q is 1 in NLS. The two soliton initial value function with and space steps $h = 0.1$, 0.05 and 0.01 and various values for the time step k and corresponding stopping times. The numerical calculation stopped when relative Hamiltonian error (= Hamiltonian at time t - Hamiltonian at time $t = 0$) was greater than 0.05 for at least 1 time unit (= twice the time for the soliton interaction).

Space step $h = 0.1$	
k	Stop
0.1 (= h)	1547
0.05 (= $h/2$)	3503
0.025 (= $h/4$)	5971
0.01 (= h^2)	610
0.009999	632
0.00999	7332
0.0099	> 30000

Space step $h = 0.05$	
k	Stop
0.05 (= h)	3766
0.025 (= $h/2$)	4132
0.0125 (= $h/4$)	14086
0.0025 (= h^2)	609
0.002499	> 30000
0.0024	

Space step $h = 0.01$	
k	Stop
0.01 (= h)	
0.005 (= $h/2$)	
0.0025 (= $h/4$)	

Table 3: The constant q is -1 in NLS. The two soliton initial value function with and space steps $h = 0.1$, 0.05 and 0.01 and various values for the time step k and corresponding stopping times. The numerical calculation stopped when relative Hamiltonian error (= Hamiltonian at time t - Hamiltonian at time $t = 0$) was greater than 0.05 for at least 1 time unit (= twice the time for the soliton interaction).

For each value h and k in Table 2, the numerical calculation ran until the relative error of the Hamiltonian remained above 0.05 for at least 1 time unit, approximately twice the time of the soliton interaction, which causes spikes in the Hamiltonian graph, see Figure 6, or until a given maximum time. Therefore the stopping time is not an exact measure of the deterioration, but a guarantee that the solution has worsened enough and is not stopped because of the spikes caused by the soliton interaction.

For positive q in the NLS, choosing k to be h^2 or smaller, resulted a high frequency oscillation free end result, as can be seen from the Table 2. However, this is no guarantee of the correctness of the numerical approximation, as can be seen from the differences in the Figure 5.

For negative q, the same stopping criteria was used, even though the soliton shape is not preserved in this case. Instead a multitude of solitons are formed. Choosing k smaller than h^2 kept the high frequency oscillations from emerging, as can be seen from the Table 3. By the time $t = 1000$ the low frequency instability has not affected the numerical runs in the case $h = 0.1$, as can be seen from the Figure 10. However, the constant interaction between solitons is bound to cause differences in the phase information and affecting the shape of the absolute value, as Figure 5 suggests.

3.2.2. Example from Weideman and Herbst [10]

As an non-soliton example we have the following initial value function for the NLS with $q = 2$:

$$u(0, x) = \frac{1}{2}(1 + \varepsilon(x, 0)),$$

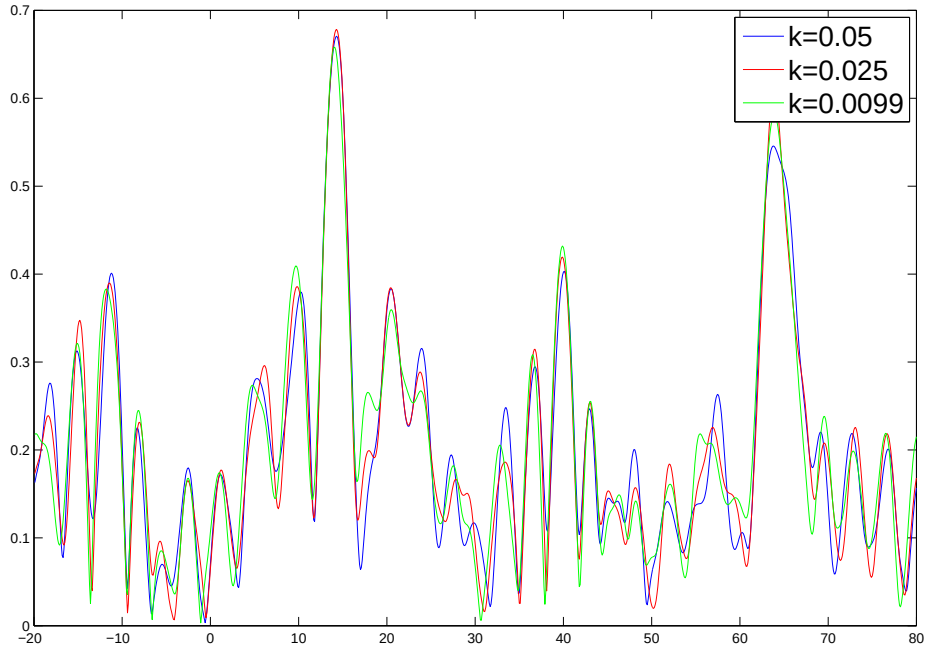

Figure 10: Three numerical runs with $q = -1$ and two soliton initial value function (25). The space step h is 0.1.

where

$$\varepsilon(x,0) = \begin{cases} 0.1(1-2x/L) & \text{, if } 0 \le x \le L/2 \\ 0.1(1+2x/L) & \text{, if } -L/2 \le x \le 0 \end{cases}$$

and where $L = 16$ and the interval is $[-8, 8]$ with periodic boundary conditions. This choice of ε gives energy into all modes. The numerical results in Table 4 confirm the necessary requirement that k has to be somewhat less than h^2. The Hamiltonian behaves similarly to the soliton case, see Figure 11.

4. Conclusions

The wave train analysis gave the restriction that the time step k should be a little smaller than h^2, the space step squared. The numerical experiments here also confirm the observed disappearance of high frequency oscillation with this choice. For the case $q < 0$ the calculation gave the limit $k < h^2$ and some limiting constant to the time and space steps. In both cases, our analysis explains the numerical results received in [1].

The numerical method conserved the incorporated ℓ^2-norm even if the solution had worsened beyond recognition. However, the growing oscillations increased the $|u_x|^2$ part of the discrete Hamiltonian which proved be an excellent indicator of a deteriorating simulation.

Acknowledgements

The authors would like to thank Uri Ascher for ideas and relevant discussion on the topic.

References

[1] U.M. Ascher, Suprising computations, Technical Report, University of British Columbia, 2009.

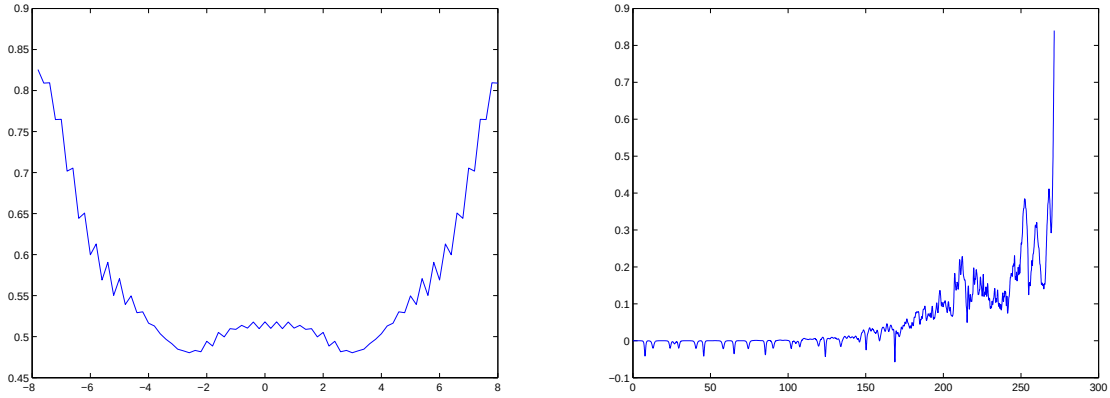

Figure 11: The approximation to $u(271, x)$ with $h = 0.2$ and $k = 0.0399$ is on the left hand side. On the right hand side is the difference between the discrete Hamiltonian at the time t and time $t = 0$.

Space step $h = 0.2$	
k	Stop
0.1 (= $h/2$)	20
0.05 (= $h/4$)	9
0.04 (= h^2)	81
0.03999	80
0.0399	271
0.039	3850
0.038	16759
0.0375	42565

Space step $h = 0.1$	
k	Stop
0.1 (= h)	33
0.05 (= $h/2$)	29
0.025 (= $h/4$)	20
0.01 (= h^2)	67
0.00999	340
0.00995	3446
0.00992	> 10000

Space step $h = 0.05$	
k	Stop
0.05 (= h)	26
0.025 (= $h/2$)	133
0.0125 (= $h/4$)	1853
0.0025 (= h^2)	133
0.002499	965
0.002495	17700
0.002493	> 30000

Table 4: The results of numerical calculations in which the initial value function is the same as the C variation in [10] with the constant function $u(0, x) = 1/2$. The calculation stopped when the relative Hamiltonian error (= Hamiltonian at time t - Hamiltonian at time $t = 0$) was greater than 0.05 for at least 1 time unit.

[2] M. Dahlby, B. Owren, Plane wave stability of some conservative schemes for the cubic Schrödinger equation, M2AN 43(4) (2009) 677687.
[3] L. Gauckler, C. Lubich, Splitting integrators for nonlinear Schrödinger equations over long times, Found. Comput. Math. 10 (2010) 275–302.
[4] W. Hundsdorfer, J.G. Verwer, Numerical solution of time-dependent advection-diffusion-reaction equations, Springer, 2003.
[5] E. Infeld, G. Rowlands, Nonlinear waves, solitons and chaos, Cambridge University Press, 1990.
[6] J.M. Sanz-Serna, Methods for the numerical solution of the nonlinear Schroedinger equation, Math. Comp. 43 (1984) 21–27.
[7] J.M. Sanz-Serna, J.G. Verwer, Conservative and nonconservative schemes for the solution of the nonlinear Schrödinger equation, IMA J. Numer. Anal. 6 (1986) 25–42.
[8] C. Sulem, P.L. Sulem, The Nonlinear Schödinger Equation: self-focusing and wave collapse, volume 139 of *Applied Mathematical Sciences*, Springer, 1999.
[9] H. Wang, Numerical studies on the split-step finite difference method for nonlinear Schrödinger equations, Appl. Math. and Comp. 170 (2005) 17–35.
[10] J.A.C. Weideman, B.M. Herbst, Split-step methods for the solution of the nonlinear schrödinger equation, SIAM J. Numer. Anal. 23(3) (1986) 485–507.
[11] V.E. Zakharov, A.B. Shabat, Exact theory of two-dimensional self-focusing and one-dimensional self-modulation of waves in nonlinear media, Soviet Physics JETP 34(1) (1972) 62–69.